State Estimation for Polyhedral Hybrid Systems and Applications to the Godunov Scheme

Jérôme Thai
Electrical Engineering and Computer Science
University of California, Berkeley
jerome.thai@berkeley.edu

Alexandre M. Bayen
Systems Engineering
University of California, Berkeley
bayen@berkeley.edu

ABSTRACT

In this article, the problem of estimating the state of a discretized hyperbolic scalar partial differential equation is studied. The discretization of the *Lighthill-Whitham-Richards* equation with a triangular flux function using the Godunov scheme is shown to lead to a hybrid linear system or *Switched Linear Systems* (SLS) with a number of modes exponential in the size of the discretized model. Some geometric properties of the partition of the space into polyhedra (in which a mode is active) are exploited to find heuristics to reduce the number of modes to a representative set. This motivates a new approach inspired from a well established technique for hybrid system estimation, namely the *interactive multiple model* (IMM). qThe performance of this new variant of the IMM is compared to the *extended Kalman filter* and the *ensemble Kalman filter* using the *Mobile Millennium* data set.

Categories and Subject Descriptors

G.1.8 [**Numerical Analysis**]: Partial Differential Equations

Keywords

Godunov Scheme, Hybrid Systems, Interactive Multiple Model

1. INTRODUCTION

Partial Differential Equations (PDEs) have been extensively used in the scientific literature because they provide a concise mathematical model to capture essential properties of a wide variety of phenomena such as fluid flow, heat, and electrodynamics. They are often used in traffic as density based traffic models. The *Lighthill-Whitham-Richards* (LWR) PDE [20, 23] and its discretization using the Godunov scheme [14, 17, 25] is a well established model for traffic dynamics, also known as the *Cell Transmission*

Model (CTM) [6, 7] in the transportation literature. State of the art traffic estimation techniques for this model include the application of the *extended Kalman filter* (EKF) to the LWR PDE by Schreiter et al. [24], and to non-scalar traffic model by Papageorgiou [22]. The application of the EKF to the LWR PDE model is problematic due to the non-differentiability of its discretization, a problem which has been partially adressed in [3] and [27]. The *ensemble Kalman filter* (EnKF) has also been applied to a velocity-based model in [29], in order to circumvent the difficulties of non-differentiability of numerical solutions to these PDEs such as the one presented in this article.

For a triangular flux function, the Godunov scheme applied to the LWR model can be proven to lead to a *piecewise affine* (PWA) hybrid system. The resulting switching-mode dynamical system combines continuous dynamics in the form of linear discretized dynamical systems, and discrete dynamics modeled by a finite automaton for the *transitions* between the modes. The problem of estimation of hybrid systems has been widely studied in past work [15, 28, 16, 1]. In particular, such techniques have been successfully used for aircraft tracking in [13] in which Bar-Shalom's *interacting multiple model* (IMM) algorithm was used [2]. Similar hybrid estimation algorithms and their applications are described in [21, 26, 12]. In the context of traffic estimation, computational difficulties arise when the IMM algorithm is applied to the highway model due to the exponential number of modes. A priori, each cell of the discretized model can be in seven different modes, which lead to 7^n modes, where n is the dimension of the state thus creating serious computational challenges in the estimation problem. One possible way to address this is with the *mixture Kalman filter* algorithm [5] which handles this complexity by randomly sampling in the space of modes.

In the present work, we approach this difficulty differently, leading to the following contributions:

- The article uses an explicit formulation of the Godunov scheme to express the evolution of the discretized LWR PDE as a PWA hybrid system

- It develops methods for reducing the number of modes to a tractable number using geometric results derived from the PWA representation of the system, and using *k-means clustering*.

- It demonstrates the performance of the method on field experiment data, and compares it to a traditional EnKF approach on the discretized LWR PDE.

Thus, the contribution of the article can be viewed as the construction of a method in which the estimation of the state of a discretized LWR PDE can be done in two steps; (1) using Kalman filtering on each of the modes written explicitly in a linear manner (which does not constitute a linearization of the dynamics like the EKF), (2) using a new framework for the mode estimation step, so it becomes tractable, which enables the use of various techniques, in particular the IMM.

The rest of the article is organized as follow: Section 2 presents the mathematical model used in the rest of the article. Section 3 unravels the PWA expression of the Godunov scheme. Section 4 presents feasible heuristics inspired from IMM using the PWA character of the Godunov scheme, and Section 4.5 presents some numerical results.

2. A HYBRID MODEL FOR THE GODUNOV SCHEME

This section briefly summarizes results derived earlier on hybrid formulations of the Godunov scheme [27]. We use the first order Godunov scheme for the discretization of the *Lighthill-Whitham-Richards* equation with a triangular flux function, and proves that the resulting nonlinear dynamical system can be decomposed in a *piecewise affine* manner. Using this explicit representation, the resulting hybrid system is shown to have an exponential number of modes.

2.1 Discretization of the LWR equation

We consider the *Lighthill-Whitham-Richards* hydrodynamic model used earlier in [27] as the distributed parameter system model of interest:

$$\frac{\partial \rho(x,t)}{\partial t} + \frac{\partial Q(\rho(x,t))}{\partial x} = 0 \qquad (2.1)$$

where $Q(\rho(x,t))$ is the flux function historically introduced by Greenshields [10]. For the rest of the work, we will instantiate the results on a triangular flux function introduced by Daganzo [7]:

$$Q_T(\rho) = \begin{cases} v_f \rho & \text{if } \rho \leq \rho_c \\ -\omega_f (\rho - \rho_{\text{jam}}) & \text{if } \rho > \rho_c \end{cases} \qquad (2.2)$$

where $\omega_f = v_f \rho_c / (\rho_{\text{jam}} - \rho_c)$ is the backwards propagation wave speed.

A seminal numerical method to solve the above equations is given by the Godunov scheme, which is based on exact solutions to Riemann problems [8, 9]. This leads to the construction of a nonlinear discrete time dynamical system. The Godunov discretization scheme is applied on the LWR PDE, where the discrete time step Δt is indexed by t, and the discrete space step Δx is indexed by i:

$$\rho_i^{t+1} = \rho_i^t - \frac{\Delta t}{\Delta x} \left(G(\rho_i^t, \rho_{i+1}^t) - G(\rho_{i-1}^t, \rho_i^t) \right) \qquad (2.3)$$

In order to ensure numerical stability, the time and space steps are coupled by the CFL condition [17]: $c_{\max} \frac{\Delta t}{\Delta x} \leq 1$ where $c_{\max}$ denotes the maximal characteristic speed.

For a triangular flux function, the Godunov flux can be expressed as the minimum of the *sending flow* $S(\rho)$ from the upstream cell and the *receiving flow* $R(\rho)$ from the downstream cell (2.4,2.5,2.6) through a boundary connecting two

cells of a homogeneous road (i.e. the upstream and downstream cells have the same characteristics). For the triangular flux function:

$$G(\rho_1, \rho_2) = \min(S(\rho_1), R(\rho_2)) \qquad (2.4)$$

$$S(\rho) = \begin{cases} Q(\rho) = v_f \rho & \text{if } \rho \leq \rho_c \\ q_c & \text{if } \rho > \rho_c \end{cases} \qquad (2.5)$$

$$R(\rho) = \begin{cases} q_c & \text{if } \rho \leq \rho_c \\ Q(\rho) = -\omega_f (\rho - \rho_{\text{jam}}) & \text{if } \rho > \rho_c \end{cases} \qquad (2.6)$$

where ρ_1 is the density of the cell upstream and ρ_2 is the density of the cell downstream.

The explicit values taken by $G(\rho_1, \rho_2)$ for a partition of the space in different regions of the space (ρ_1, ρ_2) **W**, **L**, and **D** are shown in Figure 2.1 and defined by equations 2.8. In the triangular case:

$$
G_T(\rho_1, \rho_2)
= \begin{cases} R(\rho_2) = -\omega_f (\rho_2 - \rho_{\text{jam}}) & \text{if } (\rho_1, \rho_2) \in \mathbf{W} \\ q_c & \text{if } (\rho_1, \rho_2) \in \mathbf{L} \\ S(\rho_1) = v_f \rho_1 & \text{if } (\rho_1, \rho_2) \in \mathbf{D} \end{cases} \qquad (2.7)
$$

$$
\begin{aligned}
\mathbf{W} &= \{(\rho_1, \rho_2) \mid \rho_2 > h(\rho_1) \,,\, \rho_2 > \rho_c\} \\
\mathbf{L} &= \{(\rho_1, \rho_2) \mid \rho_1 > \rho_c \,,\, \rho_2 \leq \rho_c\} \\
\mathbf{D} &= \{(\rho_1, \rho_2) \mid \rho_2 \leq h(\rho_1) \,,\, \rho_1 \leq \rho_c\}
\end{aligned} \qquad (2.8)
$$

The boundary between the **W** and **D** regions follows the $(\rho_1, \rho_2) = (\rho_1, h(\rho_1))$ trajectory for $\rho_1 \leq \rho_c$, with:[1]

$$h(\rho_1) = \bar{R}^{-1}(\bar{S}(\rho_1)) = -\frac{v_f}{\omega_f} \rho_1 + \rho_{\text{jam}} \qquad (2.9)$$

where $\bar{S}$ and $\bar{R}$ respectively denote the restrictions of the sending and receiving flows S and R to the sub-regions $[0, \rho_c)$ and $(\rho_c, \rho_{\text{jam}}]$ respectively, which also correspond to the left and right parts of the flux function (w.r.t. ρ_c), as shown in Figure 2.1.
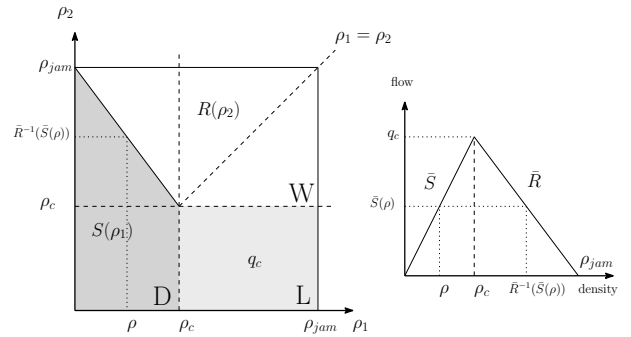
Figure 2.1: Values of $G(\rho_1, \rho_2)$ in the space (ρ_1, ρ_2).

2.2 Piecewise affine model

In the Godunov scheme (2.3), the update of the density ρ_i^{t+1} at cell i depends on the triplet $(\rho_{i-1}^t, \rho_i^t, \rho_{i+1}^t)$. With $\frac{\Delta t}{\Delta x} = \alpha$, the Godunov scheme reads:

---

[1]Here, we suppose that $\bar{R}$ is a strictly monotonic function on $(\rho_c, \rho_j]$, hence invertible, and $\bar{R}^{-1}$ denotes its inverse, which is the case for the triangular flux function.

$$\rho_i^{t+1} = \rho_i^t - \alpha \left(G(\rho_i^t, \rho_{i+1}^t) - G(\rho_{i-1}^t, \rho_i^t) \right) \qquad (2.10)$$

The expression (2.10) is non-linear but can be formulated as a *piecewise affine* hybrid system. Depending on whether (ρ_{i-1}^t, ρ_i^t) and (ρ_i^t, ρ_{i+1}^t) are in **W**, **L**, or **D**, there are nine possible combinations at cell i, which can be reduced to seven "modes" since the pairs (ρ_{i-1}^t, ρ_i^t) and (ρ_i^t, ρ_{i+1}^t) have ρ_i^t in common. Let us denote by $f(\rho_{i-1}^t, \rho_i^t, \rho_{i+1}^t)$ the vector function for the possible values of ρ_i^{t+1}. Table 2.1 lists these seven possibilities, which can be derived from Figure 2.1.

Mode	(ρ_{i-1}^t, ρ_i^t)	(ρ_i^t, ρ_{i+1}^t)	$f(\rho_{i-1}^t, \rho_i^t, \rho_{i+1}^t)$
1	**W**	**W**	$(1 - \alpha\omega_f)\rho_i^t + \alpha\omega_f\rho_{i+1}^t$
2	**W**	**L**	$(1 - \alpha\omega_f)\rho_i^t + \alpha\omega_f\rho_c$
3	**L**	**W**	$\rho_i^t + \alpha\omega_f\rho_{i+1}^t - \alpha\omega_f\rho_c$
4	**L**	**D**	$(1 - \alpha v_f)\rho_i^t + \alpha v_f\rho_c$
5	**D**	**W**	$\alpha v_f\rho_{i-1}^t + \rho_i^t + \alpha\omega_f\rho_{i+1}^t - \alpha\omega_f\rho_{\mathrm{jam}}$
6	**D**	**L**	$\alpha v_f\rho_{i-1}^t + \rho_i^t - \alpha v_f\rho_c$
7	**D**	**D**	$\alpha v_f\rho_{i-1}^t + (1 - \alpha v_f)\rho_i^t$

Table 2.1: 7×1-**dimensional column vector** $f(\rho_{i-1}^t, \rho_i^t, \rho_{i+1}^t)$ **of the different values of ρ_i^{t+1} depending on the mode.**

For example, for the first mode, (ρ_{i-1}^t, ρ_i^t) and (ρ_i^t, ρ_{i+1}^t) are both in **W** (see Figure 2.1), thus $G(\rho_{i-1}^t, \rho_i^t) = R(\rho_i^t)$ and $G(\rho_i^t, \rho_{i+1}^t) = R(\rho_{i+1}^t)$, and then $\rho_i^{t+1} = \rho_i^t - \alpha(R(\rho_{i+1}^t) - R(\rho_i^t))$. By extending this result to an entire link with discrete state space indexed by $i = 1, \cdots, n$, where n is the number of space steps, we have an exhaustive description of the space of "modes" along the link.

We define J, the Jacobian matrix of f with respect to $(\rho_{i-1}^t, \rho_i^t, \rho_{i+1}^t)$ in each of the seven modes above (which are all linear):

$$J = \left(\frac{\partial f_j}{\partial \rho_k} \right)_{j=1,\cdots,7, k=i-1,i,i+1} \qquad (2.11)$$

Where f_j is the j-th entry of the vector function f defined in Table 2.1. It is useful to make the Jacobian matrix J explicit with respect to $(\rho_{i-1}^t, \rho_i^t, \rho_{i+1}^t)$, and the constant term w:

$$J = \begin{pmatrix} 0 & 1 - \alpha\omega_f & \alpha\omega_f \\ 0 & 1 - \alpha\omega_f & 0 \\ 0 & 1 & \alpha\omega_f \\ 0 & 1 - \alpha v_f & 0 \\ \alpha v_f & 1 & \alpha\omega_f \\ \alpha v_f & 1 & 0 \\ \alpha v_f & 1 - \alpha v_f & 0 \end{pmatrix}, \; w = \begin{pmatrix} 0 \\ \alpha\omega_f\rho_c \\ -\alpha\omega_f\rho_c \\ \alpha v_f\rho_c \\ -\alpha\omega_f\rho_{\mathrm{jam}} \\ -\alpha v_f\rho_c \\ 0 \end{pmatrix}$$
$$(2.12)$$

Since f is a *linear function* of $(\rho_{i-1}^t, \rho_i^t, \rho_{i+1}^t)$ as shown in Table 2.1, we note that J is constant. More notably, the seven possible values of ρ_i^{t+1} in Table 2.1 can be rewritten in vector form as follows:

$$f(\rho_{i-1}^t, \rho_i^t, \rho_{i+1}^t) = J \begin{pmatrix} \rho_{i-1}^t \\ \rho_i^t \\ \rho_{i+1}^t \end{pmatrix} + w \qquad (2.13)$$

In the next section, we will show that the decomposition in "modes" as shown in Table 2.1 leads to a piecewise affine formulation of the Godunov scheme in the case of the triangular flux function.

Let us consider a link with discrete time step indexed by $t \geq 0$ and discrete space step indexed by $i = 1, \cdots, n$, and let us denote $\boldsymbol{\rho}^t = (\rho_0^t, \rho_1^t, \cdots, \rho_n^t, \rho_{n+1}^t)$ an $n+2$ dimensional vector which describes the state of the link at time t in the space $\mathcal{S} = [0, \rho_{\mathrm{jam}}]^{n+2}$, where ρ_i^t is the density at time t and cell i. Note that the ghost cells 0 and $n+1$ are included in the state of the link.[2]

Definition of the space of modes: Let us denote by $\mathcal{M}_n$ the space of modes of the system ($\mathcal{M}_n \subset \{1, \cdots, 7\}^n$, see Table 2.1). For $\boldsymbol{m} \in \mathcal{M}_n$, $\boldsymbol{m}$ is a vector of dimension n for which the i-th entry $m_i \in \{1, \cdots, 7\}$ is the mode at cell i. Equivalently, each element of $\mathcal{M}_n$ can be described as a sequence of regions in which the pair (ρ_i, ρ_{i+1}) is, for $i = 0, \cdots, n$. Hence, we define the equivalent space of modes $\tilde{\mathcal{M}}_n \subset \{w, l, d\}^{n+1}$, and for $\boldsymbol{s} \in \tilde{\mathcal{M}}_n$, $\boldsymbol{s}$ is a vector of dimension $n+1$ for which the i-th entry s_i is equal to l if $(\rho_i, \rho_{i+1}) \in \mathbf{L}$, for $i = 0, \cdots, n$, and similar definitions for w and d. As will be seen later, this second definition gives a description of the *partition of the space $\mathcal{S}$ into different polyhedra* $\mathbf{P_m}$ *in which the mode is* $\boldsymbol{m}$. See Figure 2.2 for an illustration.
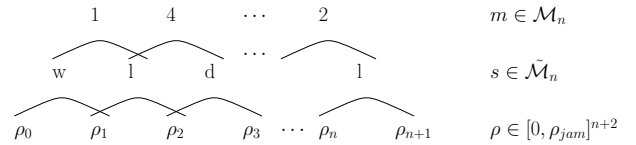
Figure 2.2: Illustration of the vectors $\boldsymbol{\rho} \in [0, \rho_{\mathbf{jam}}]^{n+2}$, $\boldsymbol{s} \in \tilde{\mathcal{M}}_n \subset \{w, l, d\}^{n+1}$, and $\boldsymbol{m} \in \mathcal{M}_n \subset \{1, \cdots, 7\}^n$ for n cells.

The n-dimensional vector $\boldsymbol{m} \in \mathcal{M}_n$ describes the mode of the link at any time, as defined in the previous section. At each time step, the state of the link is updated through the following nonlinear dynamical system:

$$\boldsymbol{\rho}^{t+1} = F_{\boldsymbol{m}}[\boldsymbol{\rho}^t] \quad \text{if} \quad \boldsymbol{\rho}^t \in \mathbf{P_m} \qquad (2.14)$$

with $F_{\boldsymbol{m}}[\cdot]$ an $n+2$ dimensional function vector, and $\boldsymbol{m}$ the mode at time t. With u^t and d^t the boundary conditions upstream and downstream at time step t, the i-th entry $\rho_i^{t+1} = F_{\boldsymbol{m},i}[\boldsymbol{\rho}^t]$ is:

$$\rho_i^{t+1} = \begin{cases} f_{m_i}(\rho_{i-1}^t, \rho_i^t, \rho_{i+1}^t) & \text{for} \quad i = 1, \cdots, n \\ u^t & \text{for} \quad i = 0 \\ d^t & \text{for} \quad i = n+1 \end{cases} \qquad (2.15)$$

where m_i denotes the i-th entry of $\boldsymbol{m} \in \mathcal{M}_n$, i.e. the mode of cell i at time step t, and $f_{m_i}(\rho_{i-1}^t, \rho_i^t, \rho_{i+1}^t)$ is the m_i-th entry of the vector-valued function f evaluated at $(\rho_{i-1}^t, \rho_i^t, \rho_{i+1}^t)$. We note that $\rho_0^{t+1} = u^t$ and $\rho_{n+1}^{t+1} = d^t$, which means that the ghost cells are the boundary conditions of the Godunov

---

[2]The values of ρ_0^t and ρ_{n+1}^t are given by the prescibed boundary conditions to be imposed on the in left and right side of the domain respectively. Note that these boundary values do not always affect the physical domain because of the nonlinear operator (2.7), which causes the boundary conditions to be implemented in the weak sense. For more details, see [29] and [25].

scheme. For a triangular flux function, with L_{m_i} the m_i-th line of J_T and w_{m_i} the m_i-th entry of w, the update operator of the dynamical system is:

$$\rho_i^{t+1} = \begin{cases} L_{m_i} \cdot \begin{pmatrix} \rho_{i-1}^t \\ \rho_i^t \\ \rho_{i+1}^t \end{pmatrix} + w_{m_i} & \text{for } i = 1, \cdots, n \\ u^t & \text{for } i = 0 \\ d^t & \text{for } i = n+1 \end{cases} \quad (2.16)$$

When $\boldsymbol{\rho}^t \in \mathbf{P_m}$, the $(n+2) \times (n+2)$-dimensional state-transition matrix $A_{\boldsymbol{m}}$ is obtained by concatenating the 3×1 row vectors L_{m_i} along the diagonal. It is tridiagonal with diagonal elements $\{0, J_{m_1,2}, \cdots, J_{m_n,2}, 0\}$, lower diagonal elements $\{J_{m_1,1}, J_{m_2,1}, \cdots, J_{m_n,1}, 0\}$, and upper diagonal elements $\{0, J_{m_1,3}, J_{m_2,3}, \cdots, J_{m_n,3}\}$ where J is defined in equation (2.12). Equivalently:

$$A_{\boldsymbol{m}} = \begin{pmatrix} 0 & \cdots & & & 0 \\ L_{m_1} & & & & \\ & & \ddots & & \\ & & & & L_{m_n} \\ 0 & \cdots & & & 0 \end{pmatrix} \quad (2.17)$$

Let us denote $b_{\boldsymbol{m}}$ and c_t the two vectors of dimension $(n+2)$ with entries $\{0, w_{m_1}, \cdots, w_{m_n}, 0\}$ and $\{u^t, 0, \cdots, 0, d^t\}$ repectively, and $\mathbf{P_m}$ the subset of space $\mathcal{S}$ where the mode is $\boldsymbol{m}$. The update operator of the dynamical system is *piecewise affine*:

$$\boldsymbol{\rho}^{t+1} = A_{\boldsymbol{m}} \boldsymbol{\rho}^t + b_{\boldsymbol{m}} + c^t \quad \text{if} \quad \boldsymbol{\rho}^t \in \mathbf{P_m} \quad (2.18)$$

We now provide a description of the partition of the space into the polyhedra $\mathbf{P_m}$ in which the mode is $\boldsymbol{m}$. Note that in this formula, $A_{\boldsymbol{m}} \boldsymbol{\rho}^t$ represents the local (affine) discretization of the PDE, and c_t the boundary condition.

2.3 Number of modes

A priori, for n cells, the number of possible modes at any given time is equal to 7^n (cf. Table 2.1). Since two consecutive indices are constrained by the evolution of equation (2.10) as derived before, the number of modes for the entire link is less than $3 \cdot (2.5)^n$.
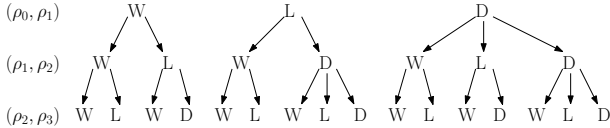
Figure 2.3: The sixteen possible modes for the first three pairs (ρ_0, ρ_1), (ρ_1, ρ_2), and (ρ_2, ρ_3).

Let n_k be the number of modes for a discretized model with k cells. Then we can recursively compute n_k with respect to k. Let us denote by w_k, l_k, and d_k the number of modes for which (ρ_k, ρ_{k+1}) is in $\mathbf{W}$, $\mathbf{L}$, and $\mathbf{D}$ respectively ($n_k = w_k + l_k + d_k$). Then these equations can be derived:

$$\begin{aligned} w_0 &= l_0 = d_0 = 1 \\ w_{k+1} &= w_k + l_k + d_k \\ l_{k+1} &= w_k + d_k \qquad \text{for } k \geq 0 \\ d_{k+1} &= l_k + d_k \end{aligned} \quad (2.19)$$

Using matrix notations and equation (2.19):

$$\begin{bmatrix} w_k \\ l_k \\ d_k \end{bmatrix} = A^k \times \begin{bmatrix} w_0 \\ l_0 \\ d_0 \end{bmatrix} \quad \text{where } A = \begin{bmatrix} 1 & 1 & 1 \\ 1 & 0 & 1 \\ 0 & 1 & 1 \end{bmatrix} \quad (2.20)$$

It is possible to compute A^k explicitly by diagonalizing the matrix A, to obtain an explicit expression for w_k, l_k, and d_k in the form of $a.\beta^k + b.\gamma^k + c.\delta^k$. However, this analytical expression is unwieldy, so we will just derive lower and upper bounds to n_k. It can be proved that $d_k \leq n_k/2$ for $k \geq 0$, then we can prove recursively that $3 \cdot 2^k \leq n_k \leq 3 \cdot (2.5)^k$.

number of cells	1	2	5	10	20
number of modes	7	16	182	10426	34206521
bound without analysis	7	49	16807	282475249	$8 \cdot 10^{16}$

Table 2.2: Number of modes for a homogeneous road.

3. HYBRID ESTIMATION ALGORITHMS

In this section, we first introduce a geometric framework for the description of the *polyhedral structure* of the hybrid system (2.18). We then develop an *interactive multiple model Kalman filter* (IMM KF) algorithm to the resulting *Polyhedral Piecewise Affine* (PPWA) hybrid system.

3.1 PPWA hybrid system

We now provide a description of the partition of the space into the polyhedra $\mathbf{P_m}$ in which the mode is $\boldsymbol{m}$. Note that in this formula, $A_{\boldsymbol{m}} \boldsymbol{\rho}^t$ represents the local (affine) discretization of the PDE, and c_t the boundary condition.

For a discretization into n cells, we chose to describe the ensemble of modes $\tilde{\mathcal{M}}_n$ in sequences $\boldsymbol{s} \in \{w, l, d\}^{n+1}$ and define $\mathbf{P_s}$ the corresponding polyhedron for each sequence. Let us define 3^{n+1} polyhedra $\mathbf{W}_i$, $\mathbf{L}_i$, and $\mathbf{D}_i$ for $i = 0, \cdots, n$ in the space $\mathcal{S}$ obtained by instantiating $h(\rho_1)$ with (2.9):

$$\begin{aligned} \mathbf{W}_i &= \{(\rho_i, \rho_{i+1}) \mid \rho_{i+1} + \tfrac{v_f}{\omega_f}\rho_i > \rho_{\text{jam}}, \ \rho_{i+1} > \rho_c\} \\ \mathbf{L}_i &= \{(\rho_i, \rho_{i+1}) \mid \rho_i > \rho_c, \ \rho_{i+1} \leq \rho_c\} \\ \mathbf{D}_i &= \{(\rho_i, \rho_{i+1}) \mid \rho_{i+1} + \tfrac{v_f}{\omega_f}\rho_i \leq \rho_{\text{jam}}, \ \rho_i \leq \rho_c\} \end{aligned} \quad (3.1)$$

The polyhedron $\mathbf{P_s}$, in which the mode is $\boldsymbol{s} \in \tilde{\mathcal{M}}_n$, can be described as an intersection of $n+1$ polyhedra $\mathbf{Q}_i$:

$$\mathbf{P_s} = \bigcap_{i=0}^{n} \mathbf{Q}_i \quad \text{with} \quad \mathbf{Q}_i = \begin{cases} \mathbf{W}_i & \text{if } s_i = w \\ \mathbf{L}_i & \text{if } s_i = l \\ \mathbf{D}_i & \text{if } s_i = d \end{cases} \quad (3.2)$$

Moreover, for two different modes $\boldsymbol{s}$ and $\boldsymbol{s}'$, and corresponding polyhedra $\mathbf{P_s} = \bigcap_{i=0}^{n} \mathbf{Q}_i$ and $\mathbf{P_{s'}} = \bigcap_{i=0}^{n} \mathbf{Q}'_i$, we can find an index i for which $\mathbf{Q}_i$ and $\mathbf{Q}'_i$ are disjoint. For instance, suppose without loss of generality that $\mathbf{Q}_i = \mathbf{W}_i$ and $\mathbf{Q}'_i = \mathbf{D}_i$, and we know that $\mathbf{W}_i$ and $\mathbf{D}_i$ are disjoint.

Then in this case, the hyperplan $\{ \boldsymbol{\rho} \mid \rho_{i+1} + \frac{v_f}{\omega_f}\rho_i = \rho_{\text{jam}} \}$ is a seperating hyperplan between $\mathbf{P}_s$ and $\mathbf{P}_{s'}$. Hence, $\mathbf{P}_s$ and $\mathbf{P}_{s'}$ are disjoint and the family $\{\mathbf{P}_s\}_{s \in \mathcal{M}_n}$ is a partition of $\tilde{\mathcal{M}}_n$.

Each polyhedron $\mathbf{P}_s$ can be defined as an intersection of a finite number of half-spaces. Such definition is called a *halfspace representation* or *H-representation* [11]. Let us introduce the following indicator functions:

$$
\begin{array}{ll}
\alpha_i(\boldsymbol{\rho}) = 1_{\{\rho_{i+1} + \frac{v_f}{\omega_f}\rho_i > \rho_{\text{jam}}\}} & \text{for } i = 0, 1, \cdots, n \\
\beta_i(\boldsymbol{\rho}) = 1_{\{\rho_i > \rho_c\}} & \text{for } i = 0, 1, \cdots, n+1
\end{array}
\tag{3.3}
$$

We define the corresponding half-spaces $\mathbf{H}_{\alpha_i}$ and $\mathbf{H}_{\beta_i}$. The complementary half-spaces $\mathcal{S} \backslash \mathbf{H}$ are denoted by $\mathbf{H}_{\alpha_i}^c$ and $\mathbf{H}_{\beta_i}^c$ and the corresponding indicator functions are $1 - \alpha_i(\boldsymbol{\rho})$ and $1 - \beta_i(\boldsymbol{\rho})$. Since we have:

$$
\begin{array}{ll}
\mathbf{W}_i & = \mathbf{H}_{\alpha_i} \cap \mathbf{H}_{\beta_{i+1}} \\
\mathbf{L}_i & = \mathbf{H}_{\beta_i} \cap \mathbf{H}_{\beta_{i+1}}^c \\
\mathbf{D}_i & = \mathbf{H}_{\alpha_i}^c \cap \mathbf{H}_{\beta_i}^c
\end{array}
\tag{3.4}
$$

for $i = 0, 1, \cdots, n$ the polyhedra defined in (3.1), their respective indicator functions are:

$$
\begin{array}{ll}
w_i(\boldsymbol{\rho}) = \alpha_i(\boldsymbol{\rho})\beta_{i+1}(\boldsymbol{\rho}) \\
l_i(\boldsymbol{\rho}) = \beta_i(\boldsymbol{\rho})(1 - \beta_{i+1}(\boldsymbol{\rho})) & \text{for } i = 0, 1, \cdots, n \\
d_i(\boldsymbol{\rho}) = (1 - \alpha_i(\boldsymbol{\rho}))(1 - \beta_i(\boldsymbol{\rho}))
\end{array}
\tag{3.5}
$$

Hence, evaluating the indicator functions $\alpha_i(\boldsymbol{\rho})$ for $i = 0, \cdots, n$, and $\beta_i(\boldsymbol{\rho})$ for $i = 0, \cdots, n+1$ gives the mode $\boldsymbol{m}$ of state $\boldsymbol{\rho}$. Equations (3.2, 3.4) give an H-representation of $\mathbf{P}_s$. With $\mathcal{H}_s$ the set of half-spaces in this representation:

$$
\mathbf{P}_s = \bigcap_{\mathbf{H} \in \mathcal{H}_s} \mathbf{H}
\tag{3.6}
$$

3.2 Kalman filter algorithm

In order to use the *Kalman filter* to estimate the state of the link given a sequence of noisy observations, we model the process by adding a white noise to the underlying dynamical system model. The "true" state at time $t + 1$, namely $\boldsymbol{\rho}^{t+1}$, is then given by the update equation:

$$
\boldsymbol{\rho}^{t+1} = A_{\boldsymbol{m}}\boldsymbol{\rho}^t + b_{\boldsymbol{m}} + c^t + \boldsymbol{\eta}^t \quad \text{if} \quad \boldsymbol{\rho}^t \in \mathbf{P}_{\boldsymbol{m}}
\tag{3.7}
$$

where $\boldsymbol{\eta}^t \sim N(0, Q^t)$ is the Gaussian zero-mean, white state noise with covariance Q^t. To apply the *control update* of the Kalman filter, it is then necessary to know the mode $\boldsymbol{m}$ of the state $\boldsymbol{\rho}^t$ (i.e. $\boldsymbol{m}$ such that $\boldsymbol{\rho}^t \in \mathbf{P}_{\boldsymbol{m}}$) by evaluating the indicator functions (3.5).

Additionally, the *observation model* for the link is given by:

$$
\boldsymbol{z}^t = H^t \boldsymbol{\rho}^t + \boldsymbol{\chi}^t
\tag{3.8}
$$

where H^t is the $p_t \times n$-dimensional linear observation matrix which encodes the p^t observations (each one of them being at a discrete cell on the discretization domain) for which the density is observed during discrete time step t, and n is the number of cells along the link. The last term in equation (3.8) is the white, zero mean observation noise $\boldsymbol{\chi}^t \sim N(0, R^t)$ with covariance matrix R^t.

Let $\hat{\boldsymbol{\rho}}^{t:t}$ and $P^{t:t}$ be the *a posteriori* state estimate and error covariance matrix at time t. The *predicted* state estimate $\hat{\boldsymbol{\rho}}_j^{t+1:t}$ and covariance estimate $P_j^{t+1:t}$ of the *prediction step* in *mode* $\boldsymbol{m}_j$ are:[3]

$$
\begin{array}{ll}
\hat{\boldsymbol{\rho}}_j^{t+1:t} & = A_{\boldsymbol{m}_j}\hat{\boldsymbol{\rho}}^{t:t} + b_{\boldsymbol{m}_j} + c^t \\
P_j^{t+1:t} & = A_{\boldsymbol{m}_j} P^{t:t}(A_{\boldsymbol{m}_j})^T + Q^t
\end{array}
\tag{3.9}
$$

The *measurement residual* $\boldsymbol{r}_j^{t+1}$, *residual covariance* S_j^{t+1}, *Kalman gain* K_j^{t+1}, *updated state estimate* $\hat{\boldsymbol{\rho}}_j^{t+1:t+1}$, and *updated estimate covariance* $P_j^{t+1:t+1}$ of the *update step* in *mode* j are:

$$
\begin{array}{ll}
\boldsymbol{r}_j^{t+1} & = \boldsymbol{z}^{t+1} - H^{t+1}\hat{\boldsymbol{\rho}}_j^{t+1:t} \\
S_j^{t+1} & = H^{t+1} P_j^{t+1:t}(H^{t+1})^T + R^{t+1} \\
K_j^{t+1} & = P_j^{t+1:t}(H^{t+1})^T (S_j^{t+1})^{-1} \\
\hat{\boldsymbol{\rho}}_j^{t+1:t+1} & = \hat{\boldsymbol{\rho}}_j^{t+1:t} + K_j^{t+1}\boldsymbol{r}_j^{t+1} \\
P_j^{t+1:t+1} & = (I - K_j^{t+1} H^{t+1})P_j^{t+1:t}
\end{array}
\tag{3.10}
$$

In [18], a measure of the likelihood of the Kalman filter in mode j is given by the *mode likelihood function* Λ_j^{t+1}, where $\mathcal{N}(x; a, b)$ is the probability density function of the normal distribution with mean a and variance b:

$$
\Lambda_j^{t+1} = \mathcal{N}(\boldsymbol{r}_j^{t+1}; \ 0, \ S_j^{t+1})
\tag{3.11}
$$

3.3 Interactive multiple model KF

Let us denote by $\boldsymbol{m}_j^t$ the event that the system is in the mode j at time t. We then assume that the model is a discrete-time stochastic linear hybrid system in which the mode evolution is governed by the finite state Markov chain

$$
\mu^{t+1} = \Pi \mu^t
\tag{3.12}
$$

where $\Pi = \{\pi_{ij}\} = P(\boldsymbol{m}_j^{t+1}|\boldsymbol{m}_i^t)$ is the mode transition matrix and $\mu^t = \{\mu_j^t\} = P(\boldsymbol{m}_j^t)$ is the mode probability at time t.

Effective estimation techniques for stochastic hybrid systems are based in multiple models since it is natural to apply a statistical filter for each of the modes. The *Interactive Multiple Model* (IMM) algorithm [2, 4, 19] is a cost-effective (in terms of performance versus complexity) estimation scheme in which there is a *mixing/interacting* step at the beginning of the estimation process, which computes new initial conditions for the Kalman filters matched to the individual modes at each time step as illustrated in Figure 3.1.

Let $\mathcal{M}^t$ be the set of modes for which the Kalman filter is applied at time step t. For the IMM algorithm, $\mathcal{M}^t = \mathcal{M}^n$ for all $t \geq 0$ since we apply the filter to every mode. The components of the *mixing* step are the *mixing probability* $\mu_{ij}^{t|t+1}$ of being in mode i at time t given that the mode at time $t + 1$ is j, the *mixed condition* $\hat{\boldsymbol{\rho}}_{0j}^{t:t}$ and $P_{0j}^{t:t}$ for the state estimate and covariance of mode j at time t, and the "spread-of-the-means" X_j in the expression of $P_{0j}^{t:t}$. They are computed for $j \in \mathcal{M}^{t+1}$ w.r.t. $\hat{\boldsymbol{\rho}}_i^{t:t}$ and $P_i^{t:t}$, the state estimate and its covariance of Kalman filter i at time t:

---

[3]Unlike in Section 2 where ρ_i and m_i denote the i-th entry of the state vector $\boldsymbol{\rho}$ and the mode $\boldsymbol{m}$ respectively, $\hat{\boldsymbol{\rho}}_j$ is the state estimate in mode $\boldsymbol{m}_j$.
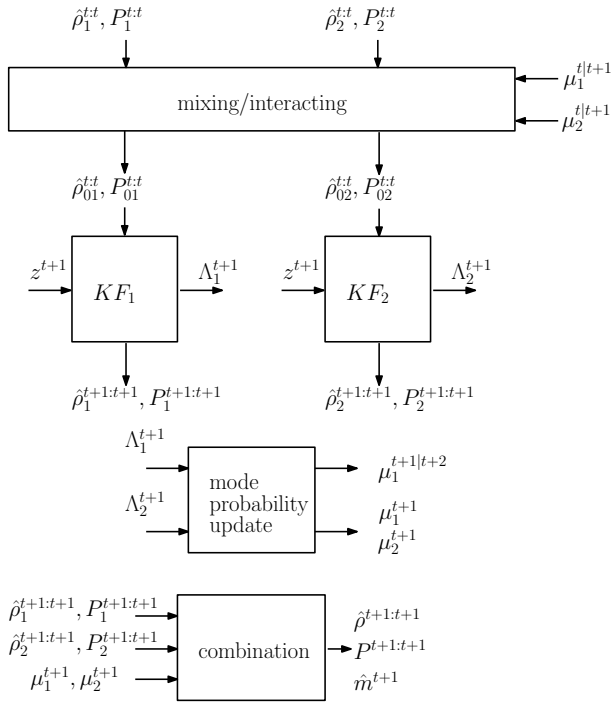
Figure 3.1: Illustration of the structure of IMM algorithm for a two-mode system from [18].

$$
\begin{aligned}
\mu_{ij}^{t|t+1} &= \tfrac{1}{Z_j}\pi_{ij}\mu_i^t \text{ for } i \in \mathcal{M}^t \\
Z_j &= \sum_{i\in\mathcal{M}^t}\pi_{ij}\mu_i^t \\
\hat{\boldsymbol{\rho}}_{0j}^{t:t} &= \sum_{i\in\mathcal{M}^t}\hat{\boldsymbol{\rho}}_i^{t:t}\mu_{ij}^{t|t+1} \\
P_{0j}^{t:t} &= \sum_{i\in\mathcal{M}^t}P_i^{t:t}\mu_{ij}^{t|t+1} + X_j \\
X_j &:= \sum_{i\in\mathcal{M}^t}(\hat{\boldsymbol{\rho}}_i^{t:t}-\hat{\boldsymbol{\rho}}_{0j}^{t:t})(\hat{\boldsymbol{\rho}}_i^{t:t}-\hat{\boldsymbol{\rho}}_{0j}^{t:t})^T\mu_{ij}^{t|t+1}
\end{aligned}
\tag{3.13}
$$

We apply the Kalman filter in each mode $j \in \mathcal{M}^{t+1}$ (KF$_j$) as described with equations (3.9,3.10) and the resulting mode likelihood functions Λ_j^{t+1} are obtained from $\hat{\boldsymbol{\rho}}_j^{t+1:t+1}$ and $P_j^{t+1:t+1}$ with equation (3.11). The mode probability $\mu^t = \{\mu_j^t\}$ is then updated through:

$$
\mu_j^{t+1} = \frac{1}{Z}\Lambda_j^{t+1}\sum_{i\in\mathcal{M}^t}\pi_{ij}\mu_i^t \text{ for } j \in \mathcal{M}^{t+1}
\tag{3.14}
$$

where Z is a normalization constant. The output of the IMM algorithm are the state estimate $\hat{\boldsymbol{\rho}}^{t+1:t+1}$ which is a weighted sum of the estimates from the Kalman filters in each mode and its covariance $P^{t+1:t+1}$, and the mode estimate $\hat{\boldsymbol{m}}^{t+1}$ is the mode which has the highest mode probability. They are given by the *combination* step:

$$
\begin{aligned}
\hat{\boldsymbol{\rho}}^{t+1:t+1} &= \sum_{j\in\mathcal{M}^{t+1}}\hat{\boldsymbol{\rho}}_j^{t+1:t+1}\mu_j^{t+1} \\
P^{t+1:t+1} &= \sum_{j\in\mathcal{M}^{t+1}}P_j^{t+1:t+1}\mu_j^{t+1} + X \\
X &:= \sum_{j\in\mathcal{M}^{t+1}}(\hat{\boldsymbol{\rho}}_j^{t+1:t+1}-\hat{\boldsymbol{\rho}}^{t+1:t+1})(\hat{\boldsymbol{\rho}}_j^{t+1:t+1}-\hat{\boldsymbol{\rho}}^{t+1:t+1})^T\mu_j^{t+1} \\
\tilde{\boldsymbol{m}}^{t+1} &:= \mathrm{argmax}_{j\in\mathcal{M}^{t+1}}\mu_j^{t+1}
\end{aligned}
\tag{3.15}
$$

In [18, 13], the IMM algorithm is used as a hybrid estimator for Air Traffic Control (ATC) tracking. The models used include one for the uniform motion and one (or more)

for the maneuver. However, the discretized PDE model described in section 2 has an exponential number of modes, as shown in Section 2.3, which induces an exponential time complexity of the IMM algorithm. Thus, the straight application of the IMM algorithm [18] as presented earlier is not tractable. The next section provides a reduced version of the algorithm, which is tractable.

4. REDUCED IMM

A solution to the tractability problem presented in the previous section consists in selecting a "representative" sample of modes following an algorithm based on the polyhedral structure of the model. Specifically, we only consider the mode in which the state estimate is and its *adjacent modes*.

4.1 Geometric properties

We extend the geometric setting presented in section 3 with definitions and the concept of *adjacent polyhedra*. We do not make any distinction between an open and closed half-space which are both denoted by $\mathbf{H}$, and the associated hyperplane is $\partial\mathbf{H}$.

Faces of a polyhedron: A supportive hyperplane of a closed convex set $\mathbf{C}$ is a hyperplane $\partial\mathbf{H}$ such as $\mathbf{C}\cap\partial\mathbf{H}\neq\emptyset$ and $\mathbf{C}\subseteq\mathbf{H}$, where $\mathbf{H}$ is one of the two half-spaces (associated to the hyperplane). Given a polyhedron $\mathbf{P}$, the inersection with any supportive hyperplane is a face of $\mathbf{P}$. Moreover, a vertex is a zero-dimension face, an edge a one-dimension face, and a facet is a face of dimension $d-1$ if $\mathbf{P}$ is of dimension d. For a full-dimensional polyhedron, a facet is of dimension $n+1$ (recall that the space $\mathcal{S}=[0,\rho_j]^{n+2}$ is of dimension $n+2$).
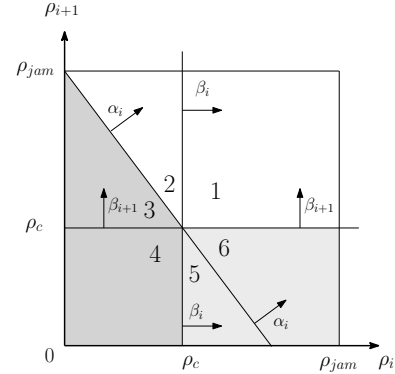
Figure 4.1: Projection of the half-spaces $\mathbf{H}_{\alpha_i}$, $\mathbf{H}_{\beta_i}$, $\mathbf{H}_{\beta_{i+1}}$, $\mathbf{H}_{\alpha_i}^c$, $\mathbf{H}_{\beta_i}^c$, $\mathbf{H}_{\beta_{i+1}}^c$ on the plan (ρ_i, ρ_{i+1}).

Minimal H-representation: There exist infinitely many H-descriptions of a convex polytope. However, for a full-dimensional convex polytope, the minimal H-description is in fact unique and is given by the set of the facet-defining halfspaces [11]. The following procedure gives the minimal H-representation of a polyhedron of the partition of $\mathcal{S}$ in our highway model.

Proposition 1: Let $\mathcal{H}_{\boldsymbol{s}}^{\min}$ be the set of half-spaces in the minimal H-representation of $\mathbf{P}_{\boldsymbol{s}}$. We have:

$$
\mathcal{H}_{\boldsymbol{s}}^{\min} \subset \left(\cup_{i=0}^n\{\mathbf{H}_{\alpha_i}, \mathbf{H}_{\alpha_i}^c\}\right) \cup \left(\cup_{i=0}^{n+1}\{\mathbf{H}_{\beta_i}, \mathbf{H}_{\beta_i}^c\}\right)
\tag{4.1}
$$

where the previous formula means family of mathematical objects as opposed to union of half-spaces. With $\mathcal{W} := \{k|s_k = w, 0 \le k \le n-1\}$, $\mathcal{L} := \{k|s_k = l, 0 \le k \le n-1\}$, $\mathcal{D} := \{k|s_k = d, 0 \le k \le n-1\}$, and $|\cdot|$ the cardinality:

$$|\mathcal{H}_{\boldsymbol{s}}^{\min}| \le 2 + |\mathcal{W}| + |\mathcal{L}| + 2 \times |\mathcal{D}| = n + 2 + |\mathcal{D}| \le 2n + 2 \quad (4.2)$$

Proof of proposition 1: The following proof gives an algorithm to find the minimal H-representation of $\mathbf{P_s}$. We have seen in section 3 that equations (3.2, 3.4) give an H-representation of $\mathbf{P_s}$ as an intersection of $2 \times (n+1)$ half-spaces, equivalently a set of $2 \times (n+1)$ inequalities. However, some of them do not define a facet of the polytope, equivalently the associated linear inequality is redundant. We want to remove such half-spaces from the H-representation $\mathcal{H}_{\boldsymbol{s}}$ and get the set $\mathcal{H}_{\boldsymbol{s}}^{\min}$ of half-spaces in the minimal H-representation of $\mathbf{P_s}$:

$$\mathbf{P_s} = \bigcap_{\mathbf{H} \in \mathcal{H}_{\boldsymbol{s}}^{\min}} \mathbf{H} \quad (4.3)$$

For this purpose, we list all the scenarios in which a half-space is redundant. They exactly happen when the intersection of two half-spaces is included in another half-space in the H-representation. There are $6 \times (n+1)$ of them as illustrated in Figure 4.1:

$$
\begin{array}{llll}
1 & \mathbf{H}_{\beta_i} \cap \mathbf{H}_{\beta_{i+1}} & \subset & \mathbf{H}_{\alpha_i} \\
2 & \mathbf{H}_{\alpha_i} \cap \mathbf{H}_{\beta_i}^c & \subset & \mathbf{H}_{\beta_{i+1}} \\
3 & \mathbf{H}_{\alpha_i}^c \cap \mathbf{H}_{\beta_{i+1}} & \subset & \mathbf{H}_{\beta_i}^c \\
4 & \mathbf{H}_{\beta_i}^c \cap \mathbf{H}_{\beta_{i+1}}^c & \subset & \mathbf{H}_{\alpha_i}^c \\
5 & \mathbf{H}_{\alpha_i}^c \cap \mathbf{H}_{\beta_i} & \subset & \mathbf{H}_{\beta_{i+1}} \\
6 & \mathbf{H}_{\alpha_i} \cap \mathbf{H}_{\beta_{i+1}}^c & \subset & \mathbf{H}_{\beta_i}
\end{array}
\quad \text{for } i = 0, \cdots, n \quad (4.4)
$$

Each triangular domain indexed from 1 to 6 in Figure 4.1 represents the intersection of the two half-spaces in each line of (4.4) respectively.projected on the plan (ρ_i, ρ_{i+1}). Then the six inclusions in (4.4) projected on (ρ_i, ρ_{i+1}) become clear and they hold in the entire space since the constraints only span on the variables ρ_i and ρ_{i+1}.

Starting from $k = 0$, we construct the sequence of sets $\{\mathcal{H}_k\}_{k=0,...,n}$ such that $\mathcal{H}_k$ is the set of half-spaces in the minimal H-representation of the polyhedron $\mathbf{P}_{\boldsymbol{s},k} = \bigcap_{i=0}^{k} \mathbf{Q}_i$ for $k = 0, ..., n$. We have $\mathcal{H}_0 = \{\mathbf{H}_0, \mathbf{H}_0'\}$ where $\mathbf{H}_0$ and $\mathbf{H}_0'$ are the two half-spaces in the minimal H-reprentation of $\mathbf{Q}_0$ given by equations (3.4). Suppose we know $\mathcal{H}_k$ and we construct $\mathcal{H}_{k+1}$ by adding only the non-redundant constraints in $\mathbf{Q}_{k+1}$. There are seven cases depending on $s(k)$ and $s(k+1)$:

Case	$s(k)$	$s(k+1)$	$\mathcal{H}_{k+1}$	$|\mathcal{H}_{k+1}|$
1	w	w	$\mathcal{H}_k \cup \{\mathbf{H}_{\beta_{k+2}}\}$	$= |\mathcal{H}_k| + 1$
2	w	l	$\mathcal{H}_k \cup \{\mathbf{H}_{\beta_{k+2}}^c\}$	$= |\mathcal{H}_k| + 1$
3	l	w	$\mathcal{H}_k \cup \{\mathbf{H}_{\alpha_{k+1}}\}$	$= |\mathcal{H}_k| + 1$
4	l	d	$\mathcal{H}_k \cup \{\mathbf{H}_{\alpha_{k+1}}^c\}$	$= |\mathcal{H}_k| + 1$
5	d	w	$\mathcal{H}_k \cup \{\mathbf{H}_{\alpha_{k+1}}, \mathbf{H}_{\beta_{k+2}}\}$	$= |\mathcal{H}_k| + 2$
6	d	l	$\mathcal{H}_k \backslash \{\mathbf{H}_{\beta_k}^c\} \cup \{\mathbf{H}_{\beta_{k+1}}, \mathbf{H}_{\beta_{k+2}}^c\}$	$\le |\mathcal{H}_k| + 2$
7	d	d	$\mathcal{H}_k \backslash \{\mathbf{H}_{\alpha_k}^c\} \cup \{\mathbf{H}_{\alpha_{k+1}}^c, \mathbf{H}_{\beta_{k+1}}^c\}$	$\le |\mathcal{H}_k| + 2$

Table 4.1: Construction of $\mathcal{H}_{k+1}$ given $\mathcal{H}_k$, and cardinality of $\mathcal{H}_{k+1}$.

For case 1 (repectively 3), the non-redundant constraint when adding $\mathbf{W}_{k+1}$ is $\mathbf{H}_{\beta_{k+2}}$ (respectively $\mathbf{H}_{\alpha_{k+1}}$) from scenario 1 (respectively 2) in (4.4). In case 2 (respectively 4), the constraint $\mathbf{H}_{\beta_{k+1}}$ (respectively $\mathbf{H}_{\beta_{k+1}}^c$) in $\mathbf{L}_{k+1}$ (respectively $\mathbf{D}_{k+1}$) is already implied by $s(k) = w$ (respectively $s(k) = l$). For case 6 (respectively 7), the constraint $\mathbf{H}_{\beta_k}^c$ (respectively $\mathbf{H}_{\alpha_k}^c$) in $\mathbf{D}_k$ becomes redundant from scenario 3 (respectively 4) in (4.4).

We have sequentially constructed $\mathcal{H}_k$ for $k = 0, \cdots, n$ and $\mathcal{H}_n = \mathcal{H}_{\boldsymbol{s}}^{\min}$ is the sef of half-spaces in the minimal H-representation of $\mathbf{P_s}$. Since the minimal H-representation is unique, this completes the proof of (4.1) and (4.2). And Table 4.1 also shows that $|\mathcal{H}_{k+1}| \le |\mathcal{H}_{k+1}| + 1$ if $s(k) \in \{w, l\}$ and $|\mathcal{H}_{k+1}| \le |\mathcal{H}_{k+1}| + 2$ if $s(k) = d$, which gives (4.2) by induction. $\square$

The polyhedra are assumed to be closed in the following definitions.

Adjacent polyhedra: Two polyhedra $\mathbf{P}$ and $\mathbf{P}'$ in a polyhedral partition of the space $\mathcal{S}$ are said to be k-*adjacent* if they have a face of dimension k in common. Formally, this is when there exists a supportive hyperplane $\partial \mathbf{H}$ for both $\mathbf{P}$ and $\mathbf{P}'$ and the intersection $\mathbf{P} \cap \mathbf{P}' \cap \partial \mathbf{H}$ is of dimension k.

$\mathbf{Q}_k$	Transformation 1	Transformation 2
$\mathbf{W}_k$	$\mathbf{H}_{\alpha_k}^c \cap \mathbf{H}_{\beta_{k+1}} \subset \mathbf{D}_k$	$\mathbf{H}_{\alpha_k} \cap \mathbf{H}_{\beta_{k+1}}^c \subset \mathbf{L}_k$
$\mathbf{L}_k$	$\mathbf{H}_{\beta_k}^c \cap \mathbf{H}_{\beta_{k+1}}^c \subset \mathbf{D}_k$	$\mathbf{H}_{\beta_k} \cap \mathbf{H}_{\beta_{k+1}} \subset \mathbf{W}_k$
$\mathbf{D}_k$	$\mathbf{H}_{\alpha_k} \cap \mathbf{H}_{\beta_k}^c \subset \mathbf{W}_k$	$\mathbf{H}_{\alpha_k}^c \cap \mathbf{H}_{\beta_k} \subset \mathbf{L}_k$

Table 4.2: Transformation of the polyhedra $\mathbf{Q}_k = \mathbf{H} \cap \mathbf{H}'$ into $\mathbf{H}^c \cap \mathbf{H}'$ for transformation 1, and into $\mathbf{H} \cap (\mathbf{H}')^c$ for transformation 2.

Proposition 2: Recall that the space $\mathcal{S} = [0, \rho_j]^{n+2}$ is of dimension $n + 2$. Given a polyhedron $\mathbf{P}_{\boldsymbol{s}_0}$ of the partition of $\mathcal{S}$, let us define the function $\mathcal{F}_{\boldsymbol{s}_0}$ from $\mathcal{H}_{\boldsymbol{s}_0}^{\min}$ the set of half-spaces in its minimal H-representation to $\mathcal{A}_{\boldsymbol{s}_0}$ the set of polyhedra of the partition $(n+1)$-adjacent to $\mathbf{P}_{\boldsymbol{s}_0}$:

$$
\mathcal{F}_{\boldsymbol{s}_0} : \quad
\begin{aligned}
\mathcal{H}_{\boldsymbol{s}_0}^{\min} &\to \mathcal{A}_{\boldsymbol{s}_0} \\
\mathbf{H} &\mapsto \mathbf{P}_{\boldsymbol{s}}
\end{aligned}
\quad (4.5)
$$

where $\boldsymbol{s}$ in $\mathcal{F}_{\boldsymbol{s}_0}[\mathbf{H}] = \mathbf{P}_{\boldsymbol{s}}$ is the unique mode $\boldsymbol{s}'$ such that

$$\left(\cap_{\mathbf{H}' \in \mathcal{H}_{\boldsymbol{s}_0} \backslash \mathbf{H}} \mathbf{H}' \right) \cap \mathbf{H}^c \subset \mathbf{P}_{\boldsymbol{s}'} \quad (4.6)$$

Then $\mathcal{F}_{\boldsymbol{s}_0}$ is a *bijection*.

Proof of proposition 2: Let us show that $\mathcal{F}_{\boldsymbol{s}_0}$ is *well-defined*. Without loss of generality, let us assume that $s_{i_0-1} = w$, $s_{i_0} = l$, and $\mathbf{H} = \mathbf{H}_{\beta_{i_0}}$, since all the other cases can be treated in a similar manner. Hence, $\mathbf{W}_{i_0-1} = \mathbf{H}_{\alpha_{i_0}-1} \cap \mathbf{H}_{\beta_{i_0}}$ and $\mathbf{L}_{i_0} = \mathbf{H}_{\beta_{i_0}} \cap \mathbf{H}_{\beta_{i_0}+1}^c$ are the only two polyhedra of the H-representation of $\mathbf{P}_{\boldsymbol{s}}$ which have $\mathbf{H}_{\beta_{i_0}}$ as a facet-defining half-space. Therefore:

$$
\begin{aligned}
& \left(\cap_{\mathbf{H}' \in \mathcal{H}_{\boldsymbol{s}_0} \backslash \mathbf{H}} \mathbf{H}' \right) \cap \mathbf{H}^c \\
&= (\cap_{i \ne i_0-1, i_0} \mathbf{Q}_i) \cap (\mathbf{H}_{\alpha_{i_0-1}} \cap \mathbf{H}_{\beta_{i_0}}^c) \cap (\mathbf{H}_{\beta_{i_0}}^c \cap \mathbf{H}_{\beta_{i_0}+1}^c) \\
&\subset (\cap_{i \ne i_0-1, i_0} \mathbf{Q}_i) \cap \mathbf{L}_{i_0-1} \cap \mathbf{D}_{i_0}
\end{aligned}
$$
$$(4.7)$$

The inclusion is obtained from Table 4.2. Hence the subset $\left(\cap_{\mathbf{H}' \in \mathcal{H}_{s_0} \setminus \mathbf{H}} \mathbf{H}'\right) \cap \mathbf{H}^c$ is included in a polyhedron of the partition $\mathbf{P_s}$. Since the subset is non empty, $\mathbf{P_s}$ is the only polyhedron containing it, and $\mathcal{F}_{s_0}(\mathbf{H}) = (\cap_{i \neq i_0-1, i_0} \mathbf{Q}_i) \cap \mathbf{L}_{i_0-1} \cap \mathbf{D}_{i_0}$ is uniquely defined. This is the only polyhedron of the partition $(n+1)$-adjacent to $\mathbf{P_s}$ with common supportive hyperplane $\partial \mathbf{H} = \partial \mathbf{H}_{\beta_{i_0}}$.

Let us show that $\mathcal{F}_{s_0}$ is *bijective*. The function $\mathcal{F}_{s_0}$ is *surjective* since it maps each of the facet-defining half-space $\mathbf{H}$ of $\mathbf{P_s}$ to the $(n+1)$-adjacent polyhedron of the partition sharing the supportive hyperplane $\partial \mathbf{H}$. And $\mathcal{F}_{s_0}$ is *injective* since for a given i and a given polyhedron $\mathbf{Q}_i$ of the H-representation, the two possible transformations of $\mathbf{Q}_i$ yield a different inclusion as shown in Table 4.2, and therefore a different adjacent polyhedron. □

4.2 Reduction to adjacent modes

We have presented in the previous section an algorithm to construct the minimal H-representation of $\hat{s}$, which enables us to find the adjacent modes of $\hat{s}$. We note that it follows from Equation (4.2) and *Proposition 2* that there are less than $2n+2$ modes adjacent to a given mode $\boldsymbol{m}$, where n is the number of cells of the discretized model. Moreover, two adjacent modes only differ by at most two entries. Hence, when the discretized model is in quasi-steady state (with only small variations between consecutive time steps), every pair of most likely active modes at time t must have adjacent elements. This suggests different heuristics for reducing the number of modes at each time step t of the IMM algorithm to a set $\mathcal{M}^t$ of cardinality linear in the dimension. In the update equations, one can exclusively consider the mode $\hat{\boldsymbol{m}}$ (or $\hat{s}$) of the state estimate $\hat{\boldsymbol{\rho}}^{t:t}$ and its adjacent modes. Hence, the number of modes considered is less than $2n+2$, and we will call this variation of the IMM algorithm the *reduced* IMM (RIMM1) algorithm.

We can further reduce the number of modes by taking into account the covariance P of the estimate and the distance between the state estimate and the facets of the polyhedron $\mathcal{P}_{\hat{s}}$. Let $\bigcap_{\mathbf{H} \in \mathcal{H}_s^{\min}} \mathbf{H}$ be the minimal H-representation of $\mathbf{P_s}$, $\partial \mathbf{H}$ the associated hyperplane, and $\mathbf{F}_H := \partial \mathbf{H} \cap \mathbf{P_s}$ the facet associated to $\mathbf{H}$. The half-spaces in the set $\mathcal{H}_s$ can be written as follows:

$$\mathbf{H} = \{\boldsymbol{\rho} \mid a_H.\boldsymbol{\rho} - b_H \leq 0\} \text{ for } \mathbf{H} \in \mathcal{H}_s \qquad (4.8)$$

Since $\mathbf{F}_H \subset \partial \mathbf{H}$, the distance between $\hat{\boldsymbol{\rho}}$ and each of the facet $\mathbf{F}_H$ is such that:

$$d(\hat{\boldsymbol{\rho}}, \mathbf{F}_H) \geq d(\hat{\boldsymbol{\rho}}, \partial \mathbf{H}) = \frac{|b_H - a_H.\hat{\boldsymbol{\rho}}|}{||a_H||} \text{ for } \mathbf{H} \in \mathcal{H}_s \quad (4.9)$$

With P the state covariance, let us define the ratio:

$$d_H(\hat{\boldsymbol{\rho}}) = \frac{d(\hat{\boldsymbol{\rho}}, \partial \mathbf{H})}{(a_H)^T P a_H} \text{ for } \mathbf{H} \in \mathcal{H}_s \qquad (4.10)$$

Thus, we only look at the adjacent modes for which $d_H(\hat{\boldsymbol{\rho}})$ is less than a given threshold *thres* (RIMM2). Intuitively, when there is a high variance $(a_H)^T P a_H$ along the direction a_H orthogonal to $\partial \mathbf{H}$, there is a higher probability that the state at the next time step is in the half-space $\mathbf{H}^c$, which is the complementary of $\mathbf{H}$, and therefore in the adjacent mode s_H with common supportive hyperplane $\partial \mathbf{H}$. We note that

this is an approximation since the projection of $\boldsymbol{\rho}$ on $\partial \mathbf{H}$ is not always on a facet of the adjacent mode s_j.

This variation on the IMM algorithm is closely related to the EKF since the Kalman filter applied in the mode $\hat{\boldsymbol{m}}$ of the state estimate $\hat{\boldsymbol{\rho}}^{t:t}$ is equivalent to linearizing around the state estimate. There is a refinement since we include the modes adjacent to $\hat{\boldsymbol{m}}$. Instead of relying on one possible active mode, we represent a set of possible modes active at time t and apply the KF to each one of them. However, the adjacent modes differ from $\hat{\boldsymbol{m}}$ by only one or two entries, and so they only represent a very restricted set of close possibilities centered around the mode estimate. As will be seen in the next section, the reduced IMM based on this reduction of modes is very similar to the EKF. An alternative approach consists in taking the most likely mode $\tilde{\boldsymbol{m}}^t = \text{argmax}_{j \in \mathcal{M}^t} \mu_j^t$, and its adjacent modes. However, this variation of the IMM algorithm fails to give a good representation of the dynamics of the discretized system. Since the mode estimate $\hat{\boldsymbol{m}}^t$ is chosen among the adjacent modes of the mode estimate $\hat{\boldsymbol{m}}^{t-1}$ at the previous time step, it differs from $\hat{\boldsymbol{m}}^{t-1}$ by at most one or two entries. However, the physical system have empirically larger variations, resulting in relatively different active modes between consecutive time steps.

4.3 Clustering of the space of modes
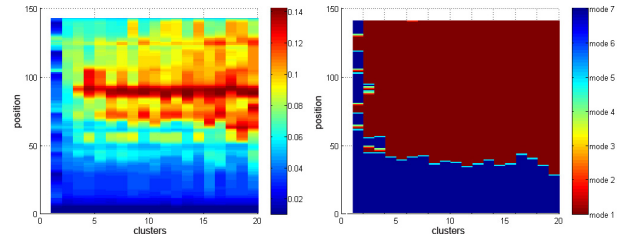
Figure 4.2: 20 clusters of the density space using *k-means* (left) and their respective modes (right).

An intuitive method to solve the latter problem consists in partitioning the space of modes $\mathcal{M}_n$ itself into K clusters with the widely-used *k-means*[4] algorithm, and transfer the adjacencies between modes studied above to the adjacencies between clusters. However, the clusters are no longer seperated by hyperplanes and additional geometrical analysis is needed to find the clusters that are close to each other. Carried further, the IMM algorithm can be applied to each of the clusters if their number K is small, and gives reasonable results (RIMM3).

Figure 4.2 shows 20 clusters of the density space. They are given by *k-means* applied to samples output by the EKF estimator using density easurements from loop detectors on March 1st, 2012 between 7am and 8am. Hence we used "historic" data to reduce the space of modes for estimation on March 5th as described in 4.5. The centroids of the partitioning of the space of modes is then given by the mode of the 20 clusters of the density space.

4.4 Analysis

It is possible to compute the *predicted state estimate* $\hat{\boldsymbol{\rho}}^{t+1:t}$ and the *predicted covariance estimate* $P^{t+1:t}$ given by (3.9)

---

[4]The *k-means* seems more adapted since it finds clusters with comparable spatial extent contrary to the *expectation-maximization* which partitions in clusters of different shapes.
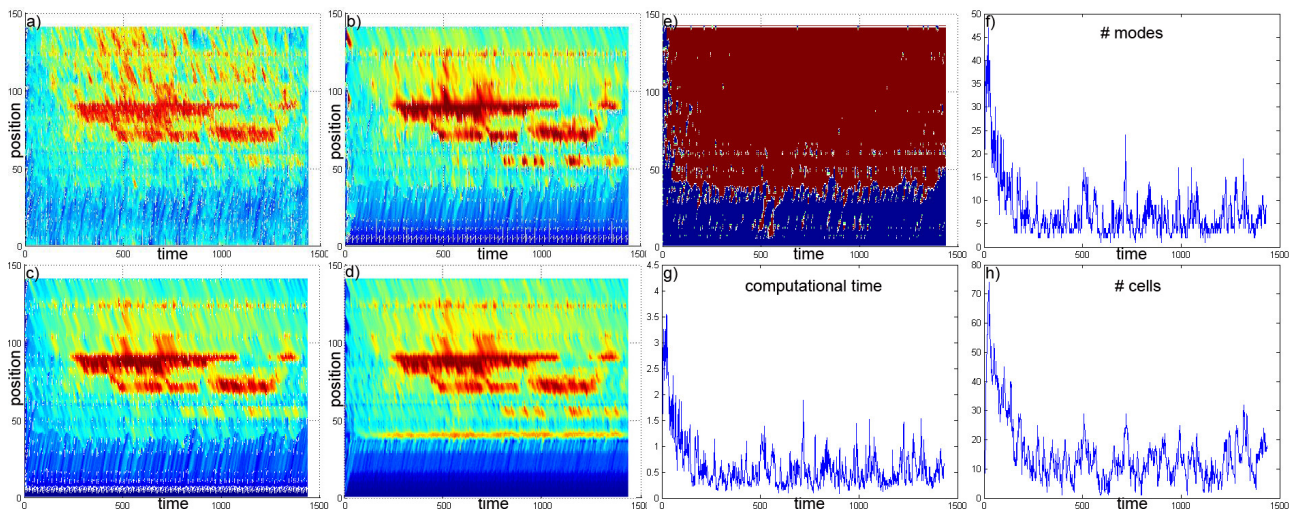
Figure 4.3: Contour plot of the density given by (a) the EnKF with 100 ensembles, (b) the EKF, (c) the RIMM2 with $thres = 1$, (d) the RIMM3 with 20 clusters using the k-means algorithm. Analysis of each time step of the RIMM2 with $thres = 1$: (e) plot of the mode estimate, (f) number of modes selected via the method of ratios, (g) computational time, (h) number of cells with density close to ρ_c.

in linear time and quadratic time respectively as shown in [27]. Hence, both time and space complexities of the *prediction step* of the Kalman filter are $O(n^2)$.

A second analysis shows that the time complexity of the *update step* of the Kalman filter is $O(mn^2 + m^3 + nm^2)$ with m the number of observations. As the density measurements along the highway are sparse, the complexity become $O(n^2)$.[5]Hence, the total complexity of the Kalman filter is $O(n^2)$.

Since the number of modes is reduced to $O(n)$, the complexity of the reduced IMM is $O(n^3)$ for both reduction heuristics presented in section 4.2. This is a significant gain from the exponential complexity of the original IMM algorithm, which considers all the modes. And if we further reduce the number of modes by restricting to the ones which have a ratio less than a threshold *thres* small enough (see equation (4.10)), then the number of.modes can be bounded. This gives a complexity $O(n^2)$.

4.5 Numerical results

The previous method is implemented on an 18-mile section of I-880 Northbound in the Bay Area, California combined with two variants of the reduced IMM estimation algorithms (RIMM2, RIMM3) presented above. We use density measurements along the I-880 from 29 loop detectors (PeMS) every 30s on March 5th, 2012 between 7am and 8am to compute density values and integrate them in the model. Each cell has a length of 198m and the time step is 5s.

The results are compared with the output of the EKF which was implemented in [27], and the output of the EnKF which is commonly used in the traffic monitoring community with this class of discretized models [29].

Figures 4.3 (a, b, c, d) present the output of the four estimators which consist in the density in the time-space domain. The regions with high density, average density,

---

[5]The measurements are sparse for our experimental data location (cf. section 4.5), but this may not be true in the general case.

and low density are represented in red, yellow, and blue respectively. The estimators give similar higher resolution scalar fields of the density (1440 time steps by 141 cells) by assimilating sparse density measurements (240 time steps by 29 PeMS stations). The shock wave propagation is more noticeable in the output of both RIMM estimators in the congested regions. Hence, these estimators are more tuned to the discretized physical system which is PWA.

Figure 4.3 (e) shows the mode estimate $\hat{s}$ computed in the *combination step* of the IMM algorithm and presented by a contour plot in the time-space domain. The regions in which $\hat{s}_i^t = w$ are in congestion and they are colored in red and the regions in which $\hat{s}_i^t = d$ are in free flow and they are represented in blue. The points of the time-space domain where $\hat{s}_i^t = l$ are colored in white and Figure 4.3 (e) shows that they are at the boundaries between the congested and free flow regions. They correspond to a regime of transition from free flow to congestion and vice versa. The estimate of the mode provided by the IMM algorithm at each point of the discretized time-space domain is thus accessible, as shown here.

Finally, Figures 4.3 (f, g, h) show that the number of modes in $\mathcal{M}^t$, the computational time, and the number of cells for which the density is close to ρ_c are highly correlated. These results show that the computational time is proportional to the number of modes. This was predictable since the application of the KF to each of the modes is the most expensive step of the IMM algorithm. This underlines the importance of reducing the number of modes to a bounded number.

5. CONCLUSION AND FUTURE WORK

A new approach in estimation of discretized hyperbolic PDEs is developed. It uses a Godunov scheme to discretize the LWR PDE with a triangular flux function. The resulting non-linear dynamical system can be decomposed in PWA components evolving with linear constraints. They partition the state space into an exponential number of polyhedra.

The initially intractable IMM becomes tractable by reducing the modes to a set of adjacent modes centered around the mode of the state estimate.

The implementation of the reduced IMM algorithm shows that it is tuned to the discretized model due to its PWA structure. The RIMM also provides an estimate of the congestion or free flow state in the time-space domain. More importantly, we have constructed a framework for the estimation of the discretized LWR PDE which enables: (1) the use of Kalman filtering on each of the linear modes, (2) the use of statistical analysis in the space of modes to make the IMM tractable.

6. ACKNOWLEDGEMENT

7. REFERENCES

[1] A. Balluchi, L. Benvenutti, M. D. di Benedetto, C. Pinello, and A. L. Sangiovanni-Vincentelli. Automative engine control and hybrid systems: challenges and opportunities. *Proc. IEEE*, 88 (7):888–912, 2000.

[2] Y. Bar-Shalom and X. R. Li. Estimation and Tracking: Principles, Techniques, and Software. *Norwood, MA: Artech House*, 1993.

[3] S. Blandin, A. Couque, A. Bayen, and D. Work. On sequential data assimilation for scalar macroscopic traffic flow models. *Physica D*, 2012.

[4] H. A. P. Blom and Y. Bar-Shalom. The interacting multiple model algorithm for systems with Markovian switching coefficients. *IEEE Trans. Autom. Control*, AC-33:780–783, August 1988.

[5] R. Chen and J. S. Liu. Mixture Kalman filters. *Royal Statistical Society*, 62:493–508, 2000.

[6] C. F. Daganzo. The cell transmission model: a dynamic representation of highway traffic consistent with the hydrodynamic theory. *Transportation Research Part B 28, no. 4*, 28:269–287, 1994.

[7] C. F. Daganzo. The cell transmission model, part II: Network traffic. *Transportation Research Part B 29, no. 2*, 29:79–93, 1995.

[8] E. Godlewski and P-A. Raviart. *Numerical approximation of hyperbolic systems of conservation laws.* Applied Mathematical Sciences, 1996.

[9] S.K. Godunov. A finite difference method for the numerical computation of discontinuous solutions of the equations of fluid dynamics. *Math. Sbornik*, 47:271–306, 1959.

[10] B. D. Greenshields. A study of traffic capacity. *Proceedings of the 14th annual meeting of the Highway Research Board*, 14:448–477, 1934.

[11] Branko Grünbaum. *Convex Polytopes.* Springer, 2003.

[12] R. M. Hawkes and J. B. Moore. Performance bounds for adaptive estimation. *Proc. IEEE*, 64:1143–1150, 1976.

[13] I. Hwang, H. Balakrishnan, and C. Tomlin. State estimation for hybrid systems: applications to aircraft tracking. *IEE Proc. Control Theory and Applications*, 153(5):556–566, Sep. 2006.

[14] J. P. Lebacque. The Godunov scheme and what it means for first order traffic flow models. *13th International Symposium on Transportation and Traffic Theory*, pages 647–77, 1996.

[15] M. D. Lemmon, K. X. He, and I. Markovsky. Supervisory hybrid systems. *IEEE Control Systems Magazine*, 19 (4):42–55, 1999.

[16] B. Lennartson, M. Tittus, B. Egardt, and S. Petterson. Hybrid systems in process control. *IEEE Control Systems Magazine*, 16 (5):45–56, 1996.

[17] R. J. LeVeque. *Numerical Methods for Conservation Laws.* Birkhäuser Basel, 1992.

[18] X. R. Li and Y. Bar-Shalom. Design of an Interacting Multiple Model Algorithm for Air Traffic Control Tracking. *IEEE Transactions on Control Systems Technology*, 1(3), September 1993.

[19] X. R. Li and Y. Bar-Shalom. Performance prediction of the interacting multiple model algorithm. *IEEE Trans. Aerosp. Electron. Syst*, 29:755–771, July 1993.

[20] M. J. Lighthill and G. B. Whitham. On Kinematic Waves II. A Theory of Traffic Flow on Long Crowded Roads. *Proceedings of the Royal Society of London. Series A, Mathematical and Physical Sciences*, 229:317–345, 1955.

[21] P. S. Maybeck. Stochastic models, estimation, and control. *Academic Press*, 2, 1982.

[22] M. Papageorgiou, J.-M. Blosseville, and H. Hadj-Salem. Modelling and real-time control of traffic flow on the southern part of Boulevard Peripherique in Paris: Part I: Modelling. *Transportation Research*, 24 (5):345–359, 1990.

[23] P. I. Richards. Shock Waves on the Highway. *Operations Research*, 4:42–51, 1956.

[24] T. Schreiter, C. van Hinsbergen, F. Zuurbier, H. van Lint, and S. Hoogendoorn. Data-model synchronization in extended Kalman filters for accurate online traffic state estimation. *2010 Proceedings of the Traffic Flow Theory Conference, Annecy, France*, 2010.

[25] I. S. Strub and A. M. Bayen. Weak formulation of boundary conditions for scalar conservation laws: an application to highway traffic modeling. *Int. J. Robust Nonlinear Control*, 16:733–748, 2006.

[26] D. D. Sworder and J. E. Boyd. Estimation problems in hybrid systems. *Cambridge University Press*, 1999.

[27] J. Thai, B. Prodhomme, and A. M. Bayen. State Estimation for the discretized LWR PDE using explicit polyhedral representations of the Godunov scheme. *In review, American Control Conference*, 2013.

[28] C. Tomlin, G. Pappas, and S. Sastry. Conflict resolution for air traffic management: A study in multiagent hybrid systems. *IEEE Trans. Autom. Control*, 43 (4), 1998.

[29] D. B. Work, S. Blandin, O. Tossavainen, B. Piccoli, and A. M. Bayen. A Traffic Model for Velocity Data Assimilation. *Applied Mathematics Research eXpress*, 2010.